Nuclear Instruments and Methods in Physics Research A 830 (2016) 338–344

Contents lists available at ScienceDirect

Nuclear Instruments and Methods in Physics Research A

journal homepage: www.elsevier.com/locate/nima

Experimental characterization of a prototype secondary spectrometer for vertically scattering multiple energy analysis at cold-neutron triple axis spectrometers

Rasmus Toft-Petersen [a,*], Felix Groitl [b,c], Mathias Kure [e,d], Joshua Lim [g], Petr Čermák [g], Svyatoslav Alimov [a], Thomas Wilpert [a], Manh Duc Le [a,f], Diana Quintero-Castro [a], Christof Niedermayer [c], Astrid Schneidewind [g], Klaus Habicht [a]

[a] Helmholtz Zentrum Berlin für Materialien und Energie GmbH, D-14109 Berlin, Germany
[b] Laboratory for Quantum Magnetism, École Polytechnique Fédérale de Lausanne, 1015 Lausanne, Switzerland
[c] Laboratory for Neutron Scattering and Imaging, Paul Scherrer Institut, 5232 Villigen, Switzerland
[d] Niels Bohr Institute, University of Copenhagen, DK-2100, Denmark
[e] Technical University of Denmark, DK-2800 Kgs., Lyngby, Denmark
[f] Institute for Basic Science (IBS), Seoul 151–747, Republic of Korea
[g] Juelich Centre for Neutron science (JCNS) at MLZ, Forschungszentrum Juelich GmbH, Outstation MLZ, Lichtenbergstr. 1, 85747 Garching, Germany

ARTICLE INFO

Article history:
Received 21 March 2016
Received in revised form
23 May 2016
Accepted 1 June 2016
Available online 3 June 2016

Keywords:
TAS
Multiplexing
Neutron spectroscopy
Inelastic neutron scattering methods
TAS spectroscopy

ABSTRACT

A thorough experimental characterization of a multiplexing backend with multiple energy analysis on a cold-neutron triple axis spectrometer (cTAS) is presented. The prototype employs two angular segments (2θ-segments) each containing five vertically scattering analyzers (energy channels), which simultaneously probe an energy transfer range of 2 meV at the corresponding two scattering angles. The feasibility and strength of such a vertically scattering multiple energy analysis setup is clearly demonstrated. It is shown, that the energy resolution near the elastic line is comparable to the energy resolution of a standard cTAS. The dispersion relation of the antiferromagnetic excitations in MnF_2 has been mapped out by performing constant energy transfer maps. These results show that the tested setup is virtually spurion free. In addition, focusing effects due to (mis)matching of the instrumental resolution ellipsoid to the excitation branch are clearly evident.

1. Introduction

There is a broad variety of scientific cases justifying importance of the parametric studies of entire dispersion surfaces. In many quantum magnets for instance a control parameter, like applied magnetic field or pressure, induce the quantum critical point [1–4]. Disordered magnetic systems also display very broad features in $\mathbf{Q}$ and ω, where excellent resolution becomes secondary to mapping capabilities [5–7]. In the past decades, triple axis spectrometers (TAS) have been optimized mainly to increase incident flux on the sample by improving guides and employing focusing monochromator and analyzer geometries. While this enhances the capability of TAS to investigate limited volumes of $(\mathbf{Q}, \omega)$-space in parametric studies, these instruments remain inefficient for overall views of the dynamic structure factor $S(\mathbf{Q}, \omega)$. Such experiments are best done on time-of-flight (ToF) spectrometers. However, sample environments for e.g. applied magnetic fields and pressure significantly limit the performance of TOF spectrometers, due to a limitation of the recorded solid angle and significant increase in background. This leaves few efficient options for parametric overview studies. A promising way to improve the $S(\mathbf{Q}, \omega)$-space coverage of a TAS is employing a multiplexing backend with several separate $(\mathbf{Q}, E_f)$-channels. Maintaining a horizontal scattering geometry for the secondary spectrometer, however, imposes physical constraints which limit solid angle coverage and also result in complex scattering geometries, such as UFO, ILL, [8,9] and RITA, PSI [10]. An impressive exception is the MACS spectrometer at NIST, that circumvents this problem by utilizing a twin analyzer concept [11]. Another way of increasing spatial angle coverage is a *vertically* scattering backend as e.g. the former Flat-Cone [12] installed at the E2 diffractometer at BER-II, Berlin, and the implemented FlatCone and the Madbox options at the ILL [13,14]. A way of increasing the mapping capabilities even further is employing a successive arrangement of vertically scattering analyzer crystals accepting multiple final energies E_f in a

* Corresponding author. Present address: Technical University of Denmark, DK-2800 Kgs., Lyngby, Denmark.
E-mail address: rasp@fysik.dtu.dk (R. Toft-Petersen).

http://dx.doi.org/10.1016/j.nima.2016.06.004
0168-9002/

single 2θ channel. This has become known as the Continuous Angle Multiple Energy Analysis (CAMEA) backend [15,16], and is possible due to the transparency of highly oriented pyrolytic graphite (HOPG) at large wavelengths [17]. This type of backend is under construction for the RITA-II cTAS at the PSI [16] and under consideration for the PANDA cTAS [18–20] at the MLZ facility [21]. In addition, this setup is to be utilized in the high performance indirect ToF spectrometer BIFROST to be built at the ESS [15]. As a BIFROST prototype the CAMEA concept has already been successfully tested on a ToF frontend [22]. Among other things this lead to the newly developed prismatic analyzer concept [23]. However, the CAMEA backend has so far not been experimentally realized with a standard cTAS frontend.

On the recently upgraded FLEXX cTAS at the HZB [24,25], a multiplexing back-end has been constructed and is under commissioning [26]. With a range of fixed vertically scattering analyzers, this optional secondary spectrometer will provide the opportunity to do overview measurements with very little effort, using less than half an hour to mechanically switch between backends. Here, the first prototype tests of the so-called MultiFLEXX multiplexing back-end, performed on the PANDA cTAS at the MLZ, are reported.

2. Prototype description

The MultiFLEXX employs 31 angular segments (2θ channels) with five fixed analyzers (energy channels) accepting final energies E_f of 2.5, 3.0, 3.5, 4.0 and 4.5 meV. This covers a range in energy-transfers of 2 meV determined by the incident neutron energy E_i. The advantages of this simple approach as opposed to more flexible backends are: no moving parts that need calibration, no motors subject to failure, the planning of an experiment and software to interpret data becomes simpler and it is feasible to interchange between classical TAS backend (analyzer and detector unit) and multiplexing backend on an experiment-to-experiment time scale. The multiplexing backend is directly attached to the sample table replacing the classical TAS secondary spectrometer.

In order to optimize the MultiFLEXX for high magnetic field sample environment with limitations on out-of-plane solid angle coverage, the out-of-plane angular coverage of the analyzers were chosen to be small (between $\pm 1.2^\circ$ and $\pm 0.7^\circ$ depending on the analyzer-sample distance). Hence, each analyzer consists of 3 vertically stacked plate-like $20 \times 20 \times 2$ mm HOPG crystals (mosaicity of $0.4^\circ \pm 0.1^\circ$ measured with x-rays), as shown in Fig. 1a. The HOPG crystals are arranged so that they have a fixed focus corresponding to their nominal fixed final energy. For each energy channel a cylindrical He-3 tube-detector with a radius of 12.5 mm and an active length of 50 mm placed 400 mm away from the center of each analyzer in the out-of-plane Bragg condition is used. The necessary detector electronics (pre-amplifiers and multi-detector interface) are directly mounted on top of the multiplexing backend. This reduces the connecting cables to a single data transfer and a single high voltage cable. These can easily follow the instrument movement during a scan. The covered angular range in 2θ is 77°, where the center of each 2θ-channel is separated by 2.5°. Taking the distances given in the caption of Fig. 1 and the analyzer dimensions into account the horizontal angular coverages of the analyzer segments with energies from 2.5 to 4.5 meV are 1.09°, 0.94°, 0.83°, 0.74° and 0.66°, respectively. With an angular separation of 2.5° between two segments the corresponding dark angles are 1.41°, 1.56°, 1.67°, 1.76° and 1.84°, respectively. This allows to completely cover the entire 2θ-range of MultiFLEXX by two scans which are separated in by $\Delta 2\theta = 1.25^\circ$.

The prototype consists of two angular segments containing 10 energy channels in total, enclosed in borated polyethylene (BPE) shielding and mounted on a table fitted with air pads (see Fig. 1b). It was mounted on the 2θ arm of the PANDA spectrometer at the MLZ. To evaluate the performance of the design three samples were used. For tests of the widths of the elastic lines a vanadium sample (diameter 1 cm, height 1 cm) was used. For a realistic evaluation of cross-talk, inelastic intensity and resolution at low energies, a 300 mg $LiMnPO_4$ $S = 5/2$ sample that orders antiferromagnetically was used [27,28]. For generating comprehensive constant energy maps and for tests of spurious signals and resolution effects, a larger MnF_2 $S = 5/2$ sample ($m \approx 30$ g) was used, exhibiting a simple antiferromagnetic spin wave spectrum with a single branch (2 ions per unit cell) [29,30]. Both magnetic samples order well above the measurement temperature of 4 K, achieved using a closed cycle cryostat ($T_N = 33.85$ K and $T_N = 67.6$ K for $LiMnPO_4$ and MnF_2, respectively).

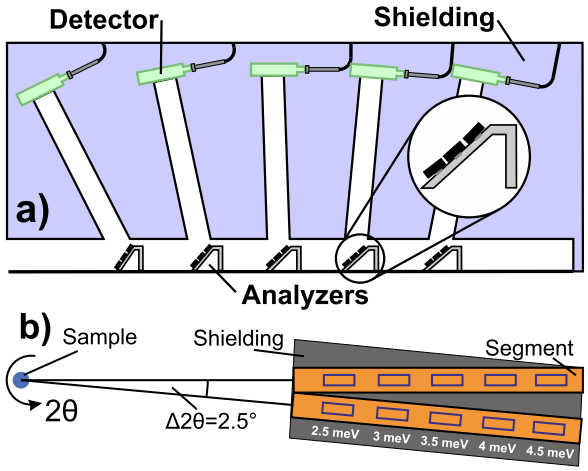

Fig. 1. (a) Layout of a single angular segment (side view), the distance between the analyzers (mounted on gray holders) and the detectors (green) is 40 cm. Neutrons scattered by the sample enter the segment from the left. The distances of the analyzers to the sample are 1050 mm, 1220 mm, 1387 mm, 1552 mm and 1732 mm, respectively. Each analyzer detector channel is thoroughly shielded with boronated polyethylene (light blue). The insert shows one analyzer (energy channel). (b) (top view) The prototype setup using two angular segments (orange) with additional shielding in between (gray) is directly attached to the sample table and replacing the classical TAS secondary spectrometer. (For interpretation of the references to color in this figure legend, the reader is referred to the web version of this article.)

3. Performance

3.1. Energy resolution

Measurements of the elastic incoherent line in vanadium probe the inherent energy resolution per distinctive energy channel. An E_i scan was performed between 2.47 (minimum E_i at PANDA for the prototype setup) and 5.2 meV. The full-width-at-half-maximum (FWHM) and peak intensities from the gaussian fits to the elastic lines are given in Table 1.

Table 1
Elastic incoherent line widths and peak intensities of a vanadium scan from 2.47 to 5.2 meV. The peak intensities have been normalized to monitor and monitor efficiency. Intensities are given in arbitrary units.

E_f	FWHM [μeV]	I_{peak}	I_{int}
2.5 meV	57(2)	3.9(1)	220(9)
3.0 meV	79(1)	4.7(1)	374(7)
3.5 meV	129(2)	3.0(1)	385(10)
4.0 meV	182(4)	1.8(1)	331(15)
4.5 meV	209(5)	1.7(1)	344(20)

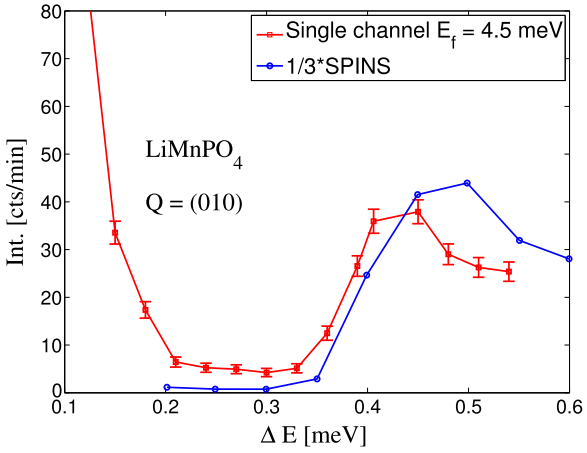

Fig. 2. Energy scan at $Q = (0\,1\,0)$ r.l.u. using the best shielded 4.5 meV channel (red), which is compared to the SPINS measurements from Ref. [28] (blue, error bars not shown). (For interpretation of the references to color in this figure legend, the reader is referred to the web version of this article.)

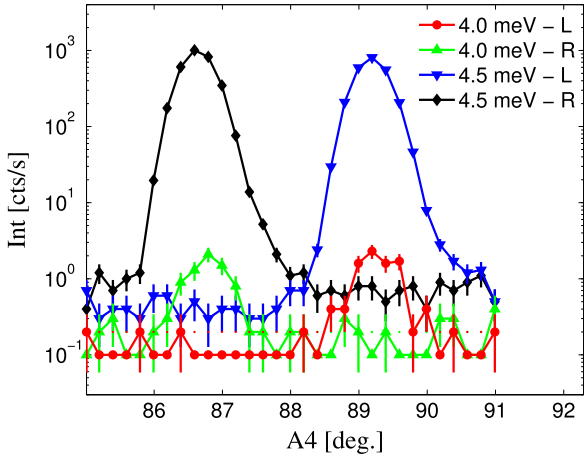

Fig. 3. *A4* scan through the (0 2 0) peak of $LiMnPO_4$ – no cross talk is evident. The indices L and R correspond to the two different cassettes. *A4* is the scattering angle of the prototype as a whole. The scattering angle 2θ of the left segment (L) is the same as *A4*, while the scattering angle of the right segment (R) has an additional offset of +2.5°. When the (0 2 0) peak is scanned over the R (L) segment, the background in the L (R) segment does not change. The 2.5, 3.0 and 3.5 meV channels all have background intensity and are not shown for clarity.

The obtained elastic incoherent line widths are comparable to, but slightly larger than the line widths expected using a horizontally arranged triple axis spectrometer at similar E_f's [19,24]. The peak intensities are larger from the low E_f analyzers closer to the sample, but the intensity is approximately constant, with the 2.5 meV channel as the exception. This is due to the fact that the increase in the volume of the resolution function, $V_{res}^{E_f} \propto k_f^3/\tan(\theta_A)$ with increasing k_f is roughly balanced out by a decrease in the volume of the resolution function due a smaller covered spatial angle further away from the sample.

In order to test the performance of the MultiFLEXX prototype near the elastic line, the gap in the excitation spectrum of $LiMnPO_4$ at $Q = (0\,1\,0)$ r.l.u. [27,28] was re-measured using a single 4.5 meV channel and a Be filter between sample and the MultiFLEXX prototype. The results are shown in Fig. 2. It is evident that a gap of 0.45 meV can easily be resolved by our setup. Ref. [28] reports a similar measurement performed on the SPINS high resolution spectrometer at NIST. A comparison of the data sets shows that the peak intensity measured on the channel furthest from the sample and normalized to time is roughly 1/3 of that measured on the SPINS spectrometer. This rather high peak intensity in one single channel clearly demonstrates the great potential of a vertically scattering multiplexing setup for cTAS.

3.2. Cross talk

Each angular segment is built as an aluminum cassette to be slid in and out of designated positions in the BPE shielding. The cassette interior is lined with a thin Cd-sheet (1 mm) to prevent cross talk. To investigate the cross talk between cassettes, the prototype containing two such cassettes was scanned across the strong (0 2 0) Bragg peak of $LiMnPO_4$ in *A4* (rotation angle of the secondary spectrometer) using a Be filter between the sample and the prototype. The results for the 4.0 and 4.5 meV channels of the two segments (L and R) are shown in Fig. 3.

The background level on the 4.5 meV channels is rather high due to elastic incoherent scattering from the sample position. However, the background in L (R) segment does not change when the (0 2 0) peak is scanned over the adjacent R (L) segment. Thus, there is virtually no cross talk between neighbored segments. For each segment there is limited intensity in the 4.0 meV channel due to the tails of the resolution function consistent with the energy width of ≈200 μeV – which will not pose a problem in inelastic measurements.

4. Investigations on the PG background

Above 15 meV, the neutron reflectivity of HOPG is markedly reduced due to parasitic Bragg reflections [31–34]. On the one hand, this allows to use HOPG as a tunable neutron filter [35–37], on the other hand it can be a severe source of unwanted background in multiplexing designs utilizing large E_i's. This effect was investigated using the very large dynamic range of the PANDA spectrometer and the fact that the 1st and 2nd order beams from the monochromator have similar intensity for typical energies [19]. Focusing on a single 2θ channel, the inelastic background was investigated by illuminating the angular segment in question with the strong (0 2 0) Bragg peak from $LiMnPO_4$ at selected energies. Elastic measurements were done for $E_i = 5$ meV (2nd order 20 meV) and $E_i = 5.5$ meV (2nd order 22 meV) without filter and for $E_i = 5.5$ meV with a PG filter mounted before the sample. The results are shown in Fig. 4. Each plot displays the signals of the energy channels for the corresponding setups.

There is significant background of several counts per second in all energy channels for the measurements without filter when sweeping over the Bragg peak in 2θ (see Fig. 4(a) and (b)). The general explanation is that the HOPG analyzer crystals act as PG filters. However, the larger background signals in the different channels, e.g. in the 2.5 meV channel (a) and in the 2.5 and 3 meV channels (b), can be linked to specific parasitic reflections using Table 4 in Ref. [32]. Using Bragg's law and the vertical scattering angles θ_A of the analyzers the energies of the parasitic reflections can be calculated. Taking into account the divergence of the beam and the PG mosaicity, the reflections which can contribute background to the performed scans are listed in Table 2. A energy difference >2 meV to the incoming energy E_i (or 2nd order) is not listed.

The strong signal in the 2.5 meV channel in Fig. 4(b) arises from 22 meV second order neutrons scattered from the (0 0 6) reflection. The background signals in all energy channels in (a, b) arise from contributions from the (1 0 6), (1 0 1) and (1 0 2) reflections. An exception is the strong signal in the 4.5 meV channel for the $E_i = 5$ meV measurement (a). Here, the analyzer still catches neutrons from the Bragg tail.

The fact that the strong background signals arise from the filter properties of the HOPG crystals is confirmed by placing a PG filter between monochromator and sample at E_i=5.5 meV (c). This

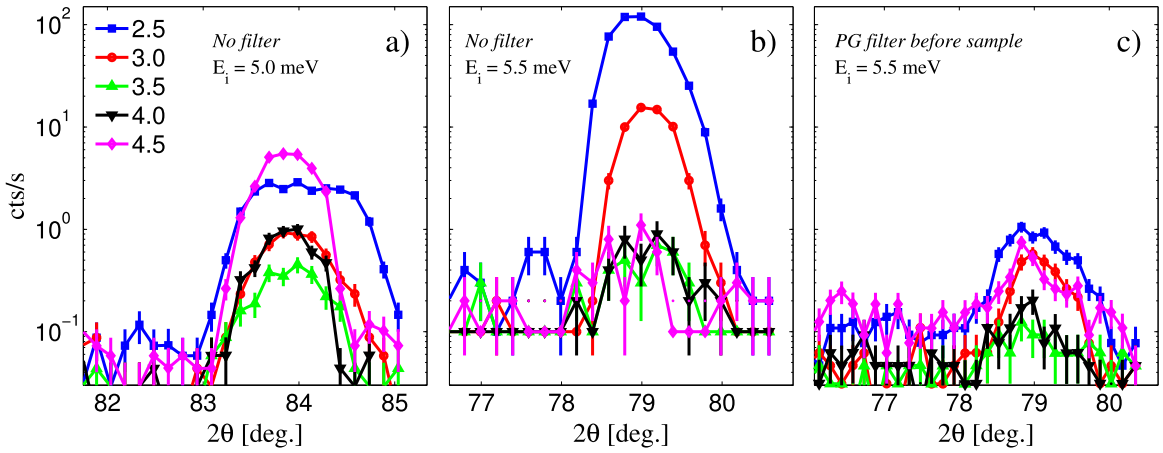

Fig. 4. Elastic 2θ scans through the (0 2 0) reflection in $LiMnPO_4$ with the intensity plotted on a logarithmic scale. Different colors display different energy channels for the scanned cassette. Measurements were performed with no filter for $E_i = 5$ meV (a) and $E_i = 5.5$ meV (b) and with PG filter before the sample for $E_i = 5.5$ meV (c). In (a) and (b) there is a unacceptable amount of inelastic background in the entire energy transfer range, which underlies the severe impact of high energy parasitic Bragg peaks on our setup as explained in the text. Using a PG filter in front of the sample (c) drastically reduces this background demonstrating, that the analyzers act as PG filters for higher incoming energies.

Table 2
Top: Vertical scattering angles θ_A for the analyzers. The analyzers are numbered in ascending order from 2.5 meV (#1) to 4.5 meV (#5). Bottom: Calculated energies reflected by the different parasitic reflections given θ_A. Energy differences >2 meV compared to the incoming energy E_i (or second order) are not listed.

Ana.	#1	#2	#3	#4	#5
θ_A [°]	58.49	51.10	46.10	42.38	39.45
Refl.	E1	E2	E3	E4	E5
[r. l. u.]	[meV]	[meV]	[meV]	[meV]	[meV]
(1 0 6)	21.04	21.77	22.71	23.67	–
(1 0 1)	–	7.15	6.44	6.03	5.77
(1 0 2)	–	7.07	6.72	6.54	6.44
(0 0 6)	22.6	–	–	–	–

greatly reduces the intensity of the 22 meV 2nd order contribution. As expected, the inelastic background drops by two orders of magnitude, confirming that HOPG analyzers can be a severe source of inelastic background at high E_i's. In addition, in a real experiment incident energies above 15 meV will produce nuclear Bragg peaks, not only from the sample but also powder peaks from unshielded parts of the sample holder and the sample environment due to the large Q-range. These strong Bragg peaks can hit one or more of the HOPG analyzers and generate large amounts of background and/or spurions.

This effect is even relevant for the MultiFLEXX in spite of the velocity selector suppressing 2nd order neutrons upstream without a Be filter between the sample and the analyzers. However, MultiFLEXX is not designed to be operated with $E_i > 10$ meV, since for these energies the incoherent elastic line will be measured as 2nd order scattering (occurring at 10, 12, 14, 16 and 18 meV) from the analyzers. However, for future CAMEA-type back ends on most cTAS this finding warrants the construction of a Be filter covering the entire 2θ range of the secondary spectrometer [38].

5. Magnetic excitations in MnF_2

The mapping capabilities of the prototype were tested by measuring the magnetic excitation of the strong scatterer MnF_2 with $S = 5/2$ and a sample volume of 8.5 cm^3 [30]. A Be filter was installed between sample and the prototype to remove 2nd order contamination (canceling effects described in the previous chapter). Such large crystals are not typical for today's spectroscopy experiments and due to the height of the sample, the energy resolution is expected to be significantly relaxed. Hence a quantitative analysis of the resolution function in the MnF_2 experiment has little value. However, the strong signal allows us to perform detailed investigations of resolution effects and prevalence of spurious signals. Furthermore, the functionality of MultiFLEXX can be demonstrated using only two angular segments out of 31 in the final design.

A normal scan procedure using the MultiFLEXX backend would include sample rotation scans (rocking scans) at different incoming neutron energies E_i. During the prototype measurements such rotation scans were repeated at different sample scattering angles 2θ to mimic a full MultiFLEXX measurement. This allowed a measurement of the spin wave dispersion evolving from the (1 0 0) Bragg peak in MnF_2 in less than 18 h using only 1/15th of the planned instrument. The rocking scans were performed for three different incident neutron energies of E_i=5.1, 5.8 and 8.5 meV resulting in a total of 15 constant energy maps, which cover almost the entire excitation spectrum as shown in Fig. 5. These maps are shown in Fig. 6. With increasing energy transfer, a clear evolution of the magnon dispersion is visible. The data is

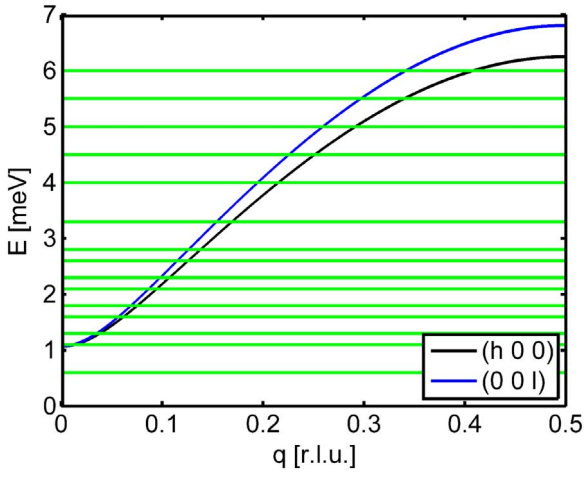

Fig. 5. The exciation spectrum of MnF_2 (black, blue) [29] is almost entirely covered by the chosen energy maps (cuts shown in green). (For interpretation of the references to color in this figure legend, the reader is referred to the web version of this article.)

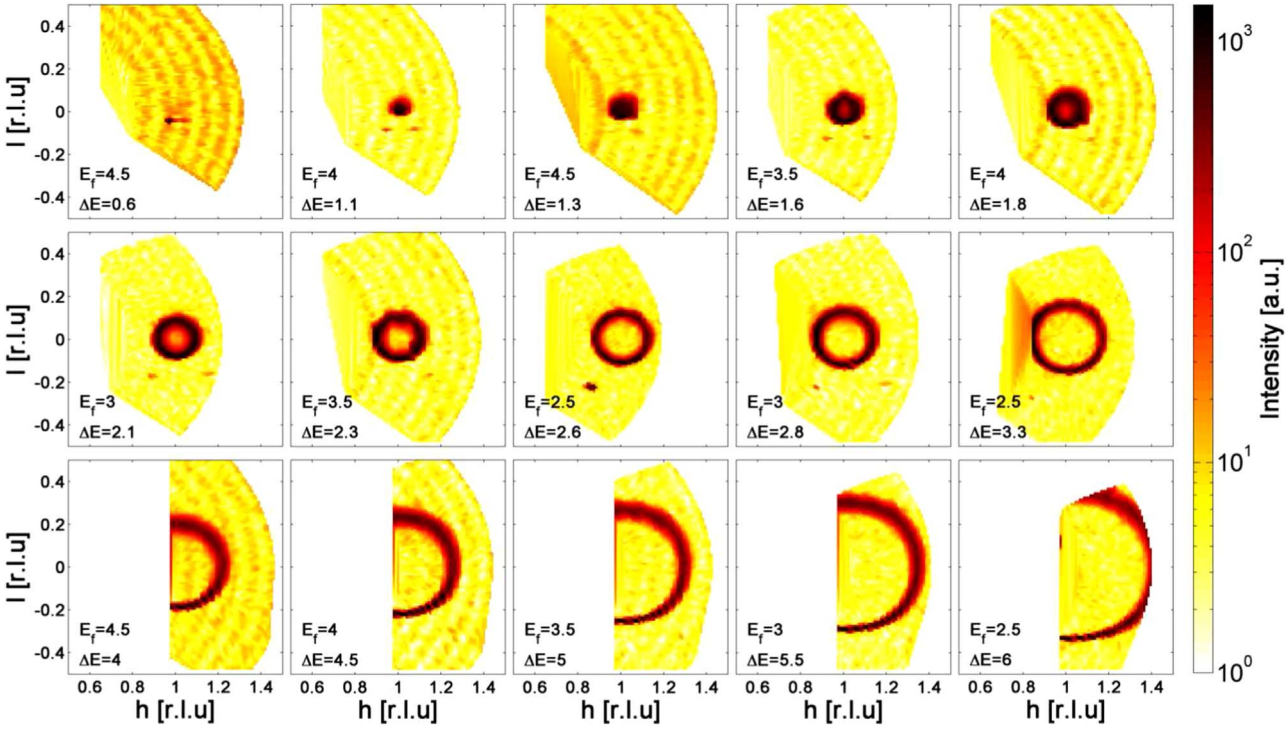

Fig. 6. Constant energy maps measured using three different incoming neutron energies. The final neutron energy as well as the energy transfer are given for each map in meV. With increasing energy transfer the evolution of the magnetic excitation out of (1 0 0) is clearly visible. The data is plotted in a logarithmic color scale to identify spurious signals.

presented on a logarithmic scale to clearly reveal spurious signals. One strong spurion is visible at $\Delta E = 2.6$ meV where the intensity of the spurion is comparable to the intensity of the inelastic excitation. Less pronounced spurions are visible for $\Delta E = 1.1$, 1.3, 1.6, 2.1 and 2.8 meV with an intensity of roughly 1/10 of the inelastic signal and all are in the same (h 0 l) region. The spurious signals arise from the strong (1 0 0) Bragg peak. Given the sample mass the intensity after the Be filter is enough to cause spurious signals above background at all analyzer segments due to the effects described in Section 4. This results in signals in all detectors, which are interpreted as an inelastic signal. Except the strong spurion in the $\Delta E = 2.6$ meV map (due to the (0 0 6) reflection, see Table 2) all spurious signals are far below the inelastic signal and would be unnoticeable with a realistic sample.

Using crystals to monochromate and analyze neutron beams for spectroscopy invariably results in tilted resolution ellipsoid when projected onto any of the (Q_i, ω), $i = x, y, z$, planes. This produces a whole range of often misinterpreted effects in measurements with a cTAS which has been subject to thorough study in the past [39–42]. The vertically scattering analyzer setup also produces resolution effects of which two are directly evident in our data. At $\Delta E = 0.6$ and $E_f = 4.5$ the energy transfer is well below the spin wave gap of 1 meV [30], yet close enough to the (1 0 0) antiferromagnetic Bragg peak for the very low energy tail of the resolution ellipsoid to graze the Bragg peak producing very localized intensity near (1, 0, −0.05). The other effect is similar to the well established focusing effect for a horizontally arranged cTAS [43]. At low energy transfers, the antiferromagnetic excitation branch is relatively flat, so the effect of the changing slope of the resolution ellipsoid at different momentum transfer is not so evident in the line shapes (see Fig. 6). However, at larger energy transfers where the resolution ellipsoid is more tilted there is a marked difference in peak width between scanning through the part of the dispersion surface where the slope of the resolution ellipsoid is focused to the dispersion and the part where the ellipsoid is defocused.

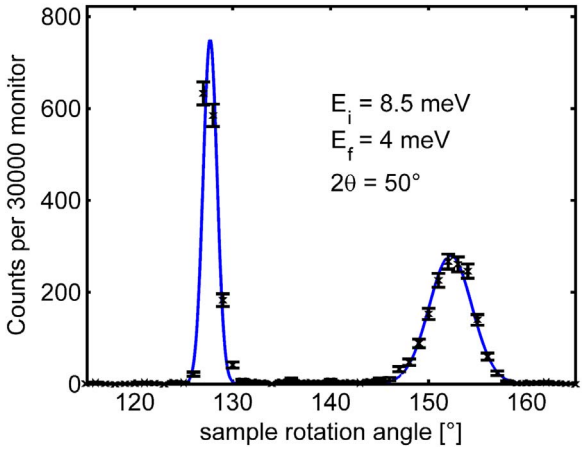

Fig. 7. Single rocking scan (θ) at $2\theta = 50°$ ($E_i = 8.5$ meV, $E_f = 3$ meV). The dispersion surface is intersected twice, once in focused condition at A3 = 127.7° (FWHM = 0.95°) and once in defocusing condition at $\theta = 152.2°$ (FWHM = 3.97°).

In Fig. 7, a sample rocking scan, that intercepts the dispersion surface twice at $\Delta E = 5.5$ meV, is shown. From the Gaussian fits to the two observed peaks the width of the focused peak is 4.2 times smaller than the unfocussed peak. This will pose a challenge for future measurements with CAMEA-type secondary spectrometers. First of all, adding data sets from equivalent parts of Q-space in high symmetry systems is more challenging than with the ToF spectrometers due to focusing effects. Secondly, in intensity limited experiments – where it will be beneficial to only focus on the parts of Q-space necessary – it will be crucial to know the resolution effects beforehand to maximize signal-to-noise ratio. Initial calculations have been made - including spatial effects – of the resolution ellipsoid of the vertically scattering flatcone setup on E2

[12]. However, a more thorough analytical understanding of the CAMEA-type resolution function, including analyzer and monochromator curvatures, will be very useful in the future where several instruments of this type will be operational.

6. Conclusion

In conclusion, extensive tests of the elastic incoherent line widths, background and inelastic resolution effects for a vertically scattering backend for cold triple axis spectrometers are presented. The elastic line widths are shown to be comparable to conventional horizontally arranged cTAS spectrometers and it is demonstrated that gaps smaller than 0.45 meV can be easily resolved using this type of setup. Although crosstalk between channels could not be detected and only few spurions were found. It was found that HOPG analyzer crystals are a major source of background at high E_i's. An extended set of constant-E maps of a large MnF_2 crystal covering a large portion of the Brillouin-zone were recorded and show that the resolution effects present in every cTAS are directly observable and prevalent in their vertically scattering counterparts.

Acknowledgments

The authors would like to thank Thomas Keller for providing the MnF_2 single crystalline sample. The authors would also like to thank Jörg Schleuer and Bernd Urban for their assistance in setting up the prototype, Jens Krüger for preparing the QMesyDAQ software for the PANDA experiment and Georg Brandl for preparing the PANDA software.

References

[1] R. Coldea, D.A. Tennant, E.M. Wheeler, E. Wawrzynska, D. Prabhakaran, M. Telling, K. Habicht, P. Smeibidl, K. Kiefer, Quantum criticality in an ising chain experimental evidence for emergent e-8 symmetry, Science 327 (5962) (2010) 177–180, http://dx.doi.org/10.1126/science.1180085.

[2] B. Lake, D.A. Tennant, J.S. Caux, T. Barthel, U. Schollwoeck, S.E. Nagler, C. D. Frost, Multispinon continua at zero and finite temperature in a near-ideal heisenberg chain, Phys. Rev. Lett. 111 (13) (2013) 137205.

[3] H. Rønnow, R. Parthasarathy, J. Jensen, G. Aeppli, T. Rosenbaum, D. McMorrow, Quantum phase transition of a magnetic in a spin bath, Science 308 (5720) (2005) 389–392.

[4] P. Merchant, B. Normand, K.W. Krämer, M. Boehm, D.F. McMorrow, C. Rüegg, Quantum and classical criticality in a dimerized quantum antiferromagnet, Nat. Phys. 10 (2014) 373–379.

[5] D.J.P. Morris, D.A. Tennant, S.A. Grigera, B. Klemke, C. Castelnovo, R. Moessner, C. Czternasty, M. Meissner, K.C. Rule, J.U. Hoffmann, K. Kiefer, S. Gerischer, D. Slobinsky, R.S. Perry, Dirac strings and magnetic monopoles in the spin ice dy2ti2o7, Science 326 (5951) (2009) 411–414.

[6] D.A. Keen, A.L. Goodwin, The crystallography of correlated disorder, Nat. Rev. 521 (2015) 303–309.

[7] J.A.M. Paddison, H. Jacobsen, O.A. Petrenko, M.T. Fernandez-Diaz, P.P. Deen, A. L. Goodwin, Hidden order in spin-liquid $Gd_3Ga_5O_{12}$, Science 350 (6257) (2015) 179–181.

[8] W. Schmidt, M.C. Rheinstaedter, S. Raymond, M. Ohl, UFO – a multi-analyser option for IN12, Phys. B – Condens. Matter 350 (1–3) (2004) E849–E851.

[9] W. Schmidt, M. Ohl, IN12-UFO: new frontiers for cold triple-axis spectroscopy, Physica B – Condensed Matter 385–386 (2006) 1073–1076; Proceedings of the 8th International Conference on Neutron Scattering, Sydney, Australia, November 27–December 02, 2005.

[10] K. Lefmann, C. Niedermayer, A.B. Abrahamsen, C.R.H. Bahl, N.B. Christensen, H. S. Jacobsen, T.L. Larsen, P. Haefliger, U. Filges, H.M. Rønnow, Realizing the full potential of a RITA spectrometer, Phys. B – Condens. Matter 385–386 (2) (2006) 1083–1085.

[11] J.A. Rodriguez, D.M. Adler, P.C. Brand, C. Broholm, J.C. Cook, C. Brocker, R. Hammond, Z. Huang, P. Hundertmark, J.W. Lynn, N.C. Maliszewskyj, J. Orndorff, D. Pierce, T.D. Pike, G. Scharfstein, S.A. Smee, R. Vilaseca, MACS – a new high intensity cold neutron spectrometer at NIST, Meas. Sci. Technol. 19 (3) (2008).

[12] D. Hohlwein, M. Kabs, K. Knorr, W. Prandl, The FlatCone diffractometer on the BER-II reactor in Berlin, Z. Kristallogr. 162 (1–4) (1983) 108–109.

[13] M. Kempa, B. Janousova, J. Saroun, P. Flores, M. Boehm, F. Demmel, J. Kulda, The FlatCone multianalyzer setup for ILL's three-axis spectrometers, Phys. B – Condens. Matter 385–386 (2) (2006) 1080–1082.

[14] F. Demmel, A. Fleischmann, W. Gläser, A multi-detector system for a triple-axis spectrometer, Nucl. Instrum. Methods Phys. Res. Sect. A – Accel. Spectrom. Detect. Assoc. Equip. 416 (1) (1998) 115–122.

[15] P.G. Freeman, J.O. Birk, M. Marko, M. Bertelsen, J. Larsen, N. B. Christensen, K. Lefmann, J. Jacobsen, C. Niedermayer, F. Juranyi, H.M. Rønnow, CAMEAESS – the continuous angle multi-energy analysis indirect geometry spectrometer for the european spallation source, in: B. Frick, M. Koza, M. Boehm, H. Mutka (Eds.), Proceedings of the QENS/WINS 2014 – 11th International Conference on Quasielastic Neutron Scattering and 6th International Workshop on Inelastic Neutron Spectrometers, Vol. 83 of EPJ Web of Conferences, EDP Sciences, 2015.

[16] F. Groitl, D. Graf, J.O. Birk, M. Markó, M. Bartkowaik, U. Filges, C. Niedermayer, C. Rüegg, H.M. Rønnow, CAMEA – a novel multiplexing analyzer for neutron spectroscopy, Rev. Sci. Instrum. 87 (2016) 035109, http://dx.doi.org/10.1063/1.4943208.

[17] J. Larsen, EPFL-report-190504, ⟨http://infoscience.epfl.ch/record/190504/files/PG_Experimental_Results_1.pdf⟩.

[18] M. Loewenhaupt, N. Pyka, Design of the triple-axis spectrometer PANDA at the high-flux reactor FRM-II of Garching, Phys. B – Condens. Matter 267 (1999) 336–340.

[19] A. Schneidewind, P. Link, D. Etzdorf, M. Rotter, M. Loewenhaupt, PANDA – first results from the cold three-axes spectrometer at FRM-II, Phys. B – Condens. Matter 385–386 (2) (2006) 1089–1091.

[20] A. Schneidewind, P. Čermák, PANDA: cold three axes spectrometer, J. Large-Scale Res. Facil. 1 (A12) (2015).

[21] J.A. Lim, K. Siemensmeyer, P. Cermak, B. Lake, A. Schneidewind, D.S. Inosov, BAMBUS: a new inelastic multiplexed neutron spectrometer for PANDA, in: M. Zhitomirsky, P. DeReotier (Eds.), Proceedings of the International Conference on Strongly Correlated Electron Systems 2014 (SCES2014), Vol. 592 of Journal of Physics Conference Series, IOP Publishing Ltd., 2015.

[22] M. Markó, EPFL-report-197952, ⟨http://infoscience.epfl.ch/record/197952/files/prototye_report_march.pdf⟩.

[23] J.O. Birk, M. Marke, P.G. Freeman, J. Jacobsen, R.L. Hansen, N.B. Christensen, C. Niedermayer, M. Mansson, H.M. Rønnow, K. Lefmann, Prismatic analyser concept for neutron spectrometers, Rev. Sci. Instrum. 85 (11) (2014).

[24] M.D. Le, D.L. Quintero-Castro, R. Toft-Petersen, F. Groitl, M. Skoulatos, K. C. Rule, K. Habicht, Nucl. Instrum. Methods Phys. Res. Sect. A – Accel. Spectrom. Detect. Assoc. Equip. 729 (2013) 220–226.

[25] M.D. Le, M. Skoulatos, D.L. Quintero-Castro, R. Toft-Petersen, F. Groitl, K. C. Rule, K. Habicht, Neutron News 25 (2014) 19–22.

[26] K. Habicht, D.L. Quintero-Castro, R. Toft-Petersen, M. Kure, L. Maede, F. Groitl, M.D. Le, The upgraded cold neutron triple-axis spectrometer FLEXX – enhanced capabilities by new instrumental options, in: B. Frick, M. Koza, M. Boehm, H. Mutka (Eds.), Proceedings of the QENS/WINS 2014 – 11th International Conference on Quasielastic Neutron Scattering and 6th International Workshop on Inelastic Neutron Spectrometers, Vol. 83 of EPJ Web of Conferences, EDP Sciences, 2015.

[27] R. Toft-Petersen, N.H. Andersen, H. Li, J. Li, W. Tian, S.L. Bud'ko, T.B.S. Jensen, C. Niedermayer, M. Laver, O. Zaharko, J.W. Lynn, D. Vaknin, Magnetic phase diagram of magnetoelectric $LiMnPO_4$, Phys. Rev. B 85 (2012) 224415.

[28] J. Li, W. Tian, Y. Chen, J.L. Zarestky, J.W. Lynn, D. Vaknin, Antiferromagnetism in the magnetoelectric effect single crystal $LiMnPO_4$, Phys. Rev. B 79 (2009) 144410.

[29] A. Okazaki, K.C. Turberfield, R.W. Stevenson, Neutron inelastic scattering measurements of antiferromagnetic excitations in MnF_2 at 4.2 K and at temperatures up to the Néel point, Phys. Lett. 8 (1964) 8.

[30] S. Bayrakci, T. Keller, K. Habicht, B. Keimer, Spin-wave lifetimes throughout the Brillouin zone, Science 312 (5782) (2006) 1926–1929.

[31] S.M. Shapiro, N.J. Chesser, Characteristics of pyrolytic graphite as an analyzer and higher order filter in neutron scattering experiments, Nucl. Instrum. Methods 101 (2) (1972) 183–186.

[32] D. Mildner, M. Arif, S. Werner, Neutron transmission through pyrolytic graphite monochromators, J. Appl. Crystallogr. 34 (3) (2001) 258–262.

[33] M. Adib, N. Habib, M. Fathaalla, Neutron transmission through pyrolytic graphite crystals, Ann. Nucl. Energy 33 (7) (2006) 627–632.

[34] M. Adib, N. Habib, I. Bashter, A. Saleh, Neutron transmission through pyrolytic graphite crystal II, Ann. Nucl. Energy 38 (4) (2011) 802–807.

[35] B. Loopstra, Neutron powder diffractometry using a Wavel 2.6 Å, Nucl. Instrum. Methods 44 (2) (1966) 181.

[36] E. Frikkee, Application of pyrolytic-graphite as a tunable neutron filter, Nucl. Instrum. Methods 125 (2) (1975) 307–312.

[37] P. Vorderwisch, U. Stuhr, S. Hautecler, Efficiency of a tunable pyrolytic graphite neutron filter, J. Neutron Res. 7 (1999) 119–129.

[38] F. Groitl, E. Rantsiou, M. Bartkowiak, U. Filges, C. Graf, D. Niedermayer, C. Rüegg, H.M. Rønnow, A combined radial collimator and cooled beryllium filter for neutron scattering, Nucl. Instrum. Methods Phys. Res. A 819 (2016) 99–103, http://dx.doi.org/10.1016/j.nima.2016.02.056.

[39] M. Cooper, R. Nathans, Resolution function in neutron diffractometry I. resolution function of a neutron diffractometer and its application to phonon measurements, Acta Crystallogr. 23 (3) (1967) 357.

[40] M. Popovici, Resolution of slow-neutron spectrometers. IV. triple-axis spectrometers resolution function, spatial effects included, Acta Crystallogr. Sect. A 31 (July 1) (1975) 507–513.

[41] J. Saroun, J. Kulda, RESTRAX – a program for TAS resolution calculation and scan profile simulation, Physica B 234 (1997) 1102–1104; Proceedings of the 1st European Conference on Neutron Scattering (ECNS 96), Interlaken, Switzerland, October 08–11, 1996.
[42] G. Eckold, O. Sobolev, Analytical approach to the 4D-resolution function of three axes neutron spectrometers with focussing monochromators and analysers, Nucl. Instrum. Methods Phys. Res. Sect. A – Accel. Spectrom. Detect. Assoc. Equip. 752 (2014) 54–64.
[43] M. Collins, Focusing effects in triple-axis neutron spectrometers, Br. J. Appl. Phys. 14 (11) (1963) 805.